



1 **Ensemble daily simulations for elucidating cloud-aerosol interactions under**
2 **a large spread of realistic environmental conditions**

3
4 **Guy Dagan¹ and Philip Stier¹**

5 ¹ Atmospheric, Oceanic and Planetary Physics, Department of Physics, University of Oxford, UK

6 E-mail: guy.dagan@physics.ox.ac.uk

7
8 **Abstract**

9 Aerosol effects on cloud properties and the atmospheric energy and radiation budgets are
10 studied through ensemble simulations over two month-long periods during the NARVAL
11 campaigns (December 2013 and August 2016). For each day, two simulations are conducted
12 with low and high cloud droplet number concentrations (CDNC), representing low and high
13 aerosol concentrations, respectively. This large data-set, which is based on a large spread of
14 co-varying realistic initial conditions, enables robust identification of the effect of CDNC
15 changes on cloud properties. We show that increases in CDNC drive a reduction in the top of
16 atmosphere (TOA) net shortwave flux (more reflection) and a decrease in the lower
17 tropospheric stability for all cases examined, while the TOA longwave flux and the liquid and
18 ice water path changes are generally positive. However, changes in cloud fraction or
19 precipitation, that could appear significant for a given day, are not as robustly affected, and, at
20 least for the summer month, are not statistically distinguishable from zero. These results
21 highlight the need for using large statistics of initial conditions for cloud-aerosol studies for
22 identifying the significance of the response. In addition, we demonstrate the dependence of the
23 aerosol effects on the season, as it is shown that the TOA net radiative effect is doubled during
24 the winter month as compared to the summer month. By separating the simulations into
25 different dominant cloud regimes, we show that the difference between the different months
26 emerge due to the compensation of the longwave effect induced by an increase in ice content
27 as compared to the shortwave effect of the liquid clouds. The CDNC effect on the longwave is
28 stronger in the summer as the clouds are deeper and the atmosphere is more unstable.

29
30
31
32
33



34 **Introduction**

35 Cloud droplets form on suitable aerosols which can serve as cloud condensation nuclei. Thus,
36 for vertical velocities which are sufficient to sustain aerosol activation, cloud droplet number
37 concentration (CDNC) increases with increasing aerosol concentrations. Concomitantly with
38 the increase in the CDNC, and assuming constant liquid water content, the initial cloud
39 hydrometeor (liquid and ice particles) size distribution shifts to smaller sizes and becomes
40 narrower, which may modulate cloud micro- and macro-physical properties (Khain et al.,
41 2005;Koren et al., 2005;Heikenfeld et al., 2019;Chen et al., 2017;Altaratz et al., 2014;Seifert
42 and Beheng, 2006a;Koren et al., 2014;Dagan et al., 2017;Dagan et al., 2018b), the rain
43 production (Levin and Cotton, 2009;Albrecht, 1989;Tao et al., 2012;Dagan et al., 2015b) and
44 the clouds' radiative effect (Koren et al., 2010;Storelvmo et al., 2011;Twomey, 1977;Albrecht,
45 1989). As the anthropogenic activity involves aerosol emissions and aerosols may influence
46 cloud radiative effects, the anthropogenic activity may perturb the Earth's radiation budget by
47 this pathway. However, despite decades of effort of trying to better understand the processes
48 involved, cloud-aerosol interactions are still considered one of the most uncertain
49 anthropogenic effects on climate (Boucher et al., 2013).

50 The aerosol effect on clouds was previously shown to be cloud regime dependent (Altaratz et
51 al., 2014;Lee et al., 2009;Mülmenstädt and Feingold, 2018;van den Heever et al.,
52 2011;Rosenfeld et al., 2013;Glassmeier and Lohmann, 2016;Gryspeerd and Stier,
53 2012;Christensen et al., 2016). In addition, even for a given cloud regime, small changes in the
54 meteorological conditions may change the sign and magnitude of the aerosol effect (Dagan et
55 al., 2015b;Fan et al., 2009;Fan et al., 2007;Kalina et al., 2014;Khain et al., 2008;Liu et al.,
56 2019).

57 The fact that the aerosol effect on clouds and precipitation is dependent on the cloud regime
58 and meteorological conditions, makes the quantification of its global effect challenging and
59 uncertain (Mülmenstädt and Feingold, 2018;Bellouin et al., 2019). One way to overcome this
60 challenge is by examining the aerosol effect for an ensemble of realistic co-varying initial
61 conditions (as opposed to perturbing each environmental condition separately). This can be
62 done by conducting ensemble/routine numerical simulations (such as those conducted in
63 previous studies (Gustafson Jr and Vogelmann, 2015;Gustafson et al., 2017;Klocke et al.,
64 2017)) focusing on aerosol effects. This methodology enables identifying, using large statistics,
65 clouds and radiative properties that respond in a consistent manner to aerosol (noting that in a
66 single-case studies some of the differences between different simulations could be just due to
67 different realizations of the model (Grabowski, 2015)). This methodology also enables



68 investigation of the aerosol effect on cloud and precipitation as a function of the initial
69 conditions.

70 In a recent paper, focusing on two specific cases (each one for two days) and a relatively large
71 domain ($22^\circ \times 11^\circ$), the physical processes controlling the aerosol effect on the atmospheric
72 energy budget were investigated (Dagan et al., 2019). It was shown that the total column
73 atmospheric radiative warming ($Q_R = (F_{SW}^{TOA} - F_{SW}^{SFC}) + (F_{LW}^{TOA} - F_{LW}^{SFC})$), defined as the rate of net
74 atmospheric diabatic warming due to radiative shortwave (SW) and longwave (LW) fluxes at
75 the surface (SFC) and top of the atmosphere (TOA), when all fluxes positive downwards), is
76 substantially increased with CDNC in a deep-cloud dominated case (by $\sim 10 \text{ W/m}^2$), while a
77 much smaller increase ($\sim 1.6 \text{ W/m}^2$) is shown in a shallow-cloud dominated case. This trend is
78 caused by an increase in the upward mass flux of ice and water vapor to the upper troposphere
79 that leads to reduced outgoing longwave radiation. The increase in mass flux is caused partially
80 by an increase in vertical velocities (Koren et al., 2005; Rosenfeld et al., 2008; Dagan et al.,
81 2018a) and mostly by an increase in the water content at the mid-troposphere (due to warm
82 rain suppression) that increases the upward mass flux, even for a give vertical velocity. The
83 change in net radiative fluxes at the TOA (F_{SW+LW}^{TOA}) was shown to be -5.2 W/m^2 for the shallow-
84 cloud dominated case and -1.9 W/m^2 for the deep-cloud dominated case. Dagan et al. (2019)
85 also show that the cloud fraction responds in opposite ways to CDNC perturbations in the
86 different cases, increasing in the deep-cloud dominated case and decreasing in the shallow-
87 cloud dominated case. However, it is unclear how representative these results are as they are
88 based on two specific cases. The ensemble simulations presented in this study could be used to
89 examine the robustness of these aerosol effects using large statistics.

90 The focus of this study is on clouds over the Atlantic Ocean near Barbados (Fig. 1). Barbados
91 is located north of the mean intertropical convergence zone (ITCZ) location, in a way that
92 samples both the trade region, dominated by shallow cumulus during the boreal winter, and the
93 transition to deep convection as the ITCZ migrates northward during boreal summer (Stevens
94 et al., 2016). Hence, this location enables investigation of different cloud regimes and different
95 meteorological conditions. In addition, the clouds near Barbados have been shown to be
96 representative of clouds across the trade region (Medeiros and Nuijens, 2016).

97

98 **Methodology**

99 Ensemble daily simulations using the icosahedral nonhydrostatic (ICON) atmospheric model
100 (Zängl et al., 2015) in a limited area configuration are conducted. ICON's dynamical core has
101 been validated against several idealized cases as well as against numerical weather prediction



skill scores (Zängl et al., 2015). The domain is located east of Barbados island and covers $\sim 3^\circ$ x 3° (Fig. 1). The simulations are aligned with the NARVAL (Next-generation Aircraft Remote-Sensing for Validation Studies (Klepp et al., 2014; Stevens et al., 2019; Stevens et al., 2016)) campaigns which took place during December 2013 (NARVAL 1) and August 2016 (NARVAL 2) in the northern tropical Atlantic. We use existing NARVAL convection-permitting simulations (Klocke et al., 2017) as initial and boundary conditions for our simulations and a two-moment bulk microphysical scheme (Seifert and Beheng, 2006b). For each day during these two months, two different simulations are started with identical initial conditions with different CDNC of 20 cm^{-3} (clean) and 200 cm^{-3} (polluted), resulting in an ensemble of 124 simulations. The different CDNC scenarios serve as proxy for different aerosol concentration conditions and are chosen as they represent the range typically observed over the ocean (Rosenfeld et al., 2019; Gryspeerd et al., 2019). Using a fixed CDNC avoid the uncertainties involved in the representation of the aerosols processes in numerical models (Rothenberg et al., 2018), however, it limits potential feedbacks between clouds and aerosols, such as through involve with aerosol scavenging.

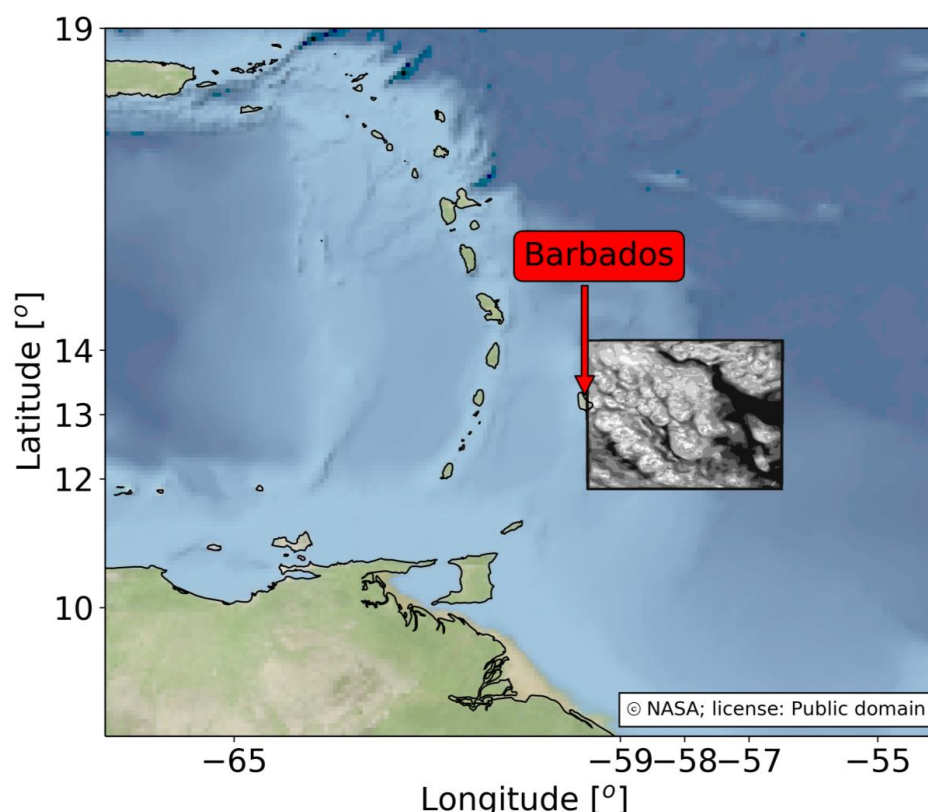
Each simulation is conducted for 24 hours starting from 12 UTC (12 hours after the original simulations of Klocke et al., 2017 started to reduce spin-up effects). The horizontal resolution is set to 1200 m and 75 vertical levels are used. The temporal resolution is 12 seconds and the output interval is 30 minutes. Interactive radiation is calculated every 12 minutes using the RRTM-G scheme (Clough et al., 2005; Iacono et al., 2008; Mlawer et al., 1997). The simulations include an interactive surface flux scheme and a fixed (for each day) sea surface temperature. As in Dagan et al. (2019), the simulations include representation of the Twomey effect, calculated with diagnosed cloud droplet effective radii from the microphysical scheme (Twomey, 1977). However, due to the large uncertainty involved in the ice microphysics and morphology, no Twomey effect due to changes in the ice particles size distribution was considered.

In addition, the domain is setup to include the Barbados Cloud Observatory (BCO, (Stevens et al., 2016)) while minimising the island effect of Barbados (most of the domain is east of the island and only the east part of the island, which includes the BCO (13°N , 59°W), is included in the domain). Observations from the BCO are used for model evaluation (Figs. S1 and S2, supporting information), and demonstrate that the model performs well for low surface-SW-flux days but underestimates the flux for high-SW-flux days (usually under low cloud fraction). We note that although a 3° x 3° domain is larger than the domains used in many previous studies, it is still possible that the use of fixed boundary conditions for the different simulations



under different CDNC conditions reduces some of the sensitivity as compared to simulations with larger domains such as in Dagan et al. (2019) ($22^\circ \times 11^\circ$). Hence, the aerosol response we present here is estimated as the lower bound.

139



140

141 **Figure 1.** The domain of the simulations (the box in the middle) and the area around it. Inside the domain
 142 is presented the average cloud fraction over the first 30 mins of the simulation for 1/8/2016, CDNC = 20
 143 cm^{-3} . The island of Barbados is marked with a red arrow.

144

145 **Results**

146 Conducting daily simulations over two months at different seasons allows us to sample a large
 147 ensemble of initial conditions and cloud types (see Fig. 2 and Table 1). To identify statistically
 148 significant differences between the two months, we conduct independent t-test (p-values are
 149 presented in Table 1). This demonstrates that the lower tropospheric stability (LTS), top of
 150 atmosphere shortwave flux (F_{SW}^{TOA}), and the atmospheric column radiative term (Q_R) are different



in a statistically significant manner (p -value < 0.05) between the two different months. The differences in other parameters are not statistically significant (Table 1).

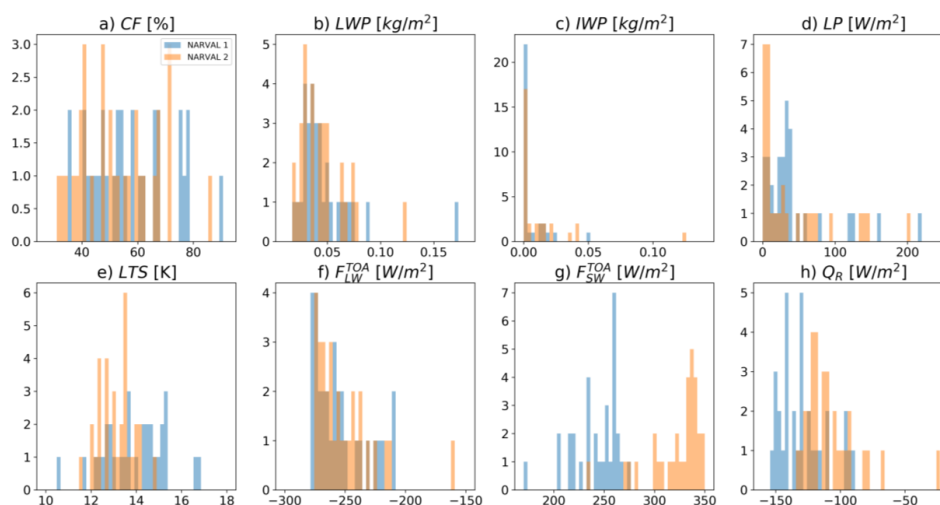


Figure 2. Histograms of mean (time and space) cloud and atmospheric properties for the base simulations with $\text{CDNC} = 20 \text{ cm}^{-3}$ (clean simulations) for each day of the two months that were simulated. Blue represents the NARVAL 1 month (December 2013), while orange the NARVAL 2 month (August 2016). a) cloud fraction – CF, b) liquid water path – LWP, c) ice water path – IWP, d) precipitation latent heat flux – LP, e) lower tropospheric stability – LTS, f) top of atmosphere longwave flux – $F_{\text{LW}}^{\text{TOA}}$, g) top of atmosphere shortwave flux – $F_{\text{SW}}^{\text{TOA}}$, and h) atmospheric column radiative term – Q_R .

Table 1. The monthly mean value of each of the properties presented in Fig. 2 ± 1 standard deviation for each month and the p -value of the two-sample independent t -test. The p -values which demonstrate a significant difference between the months (< 0.05) are presented in bold.

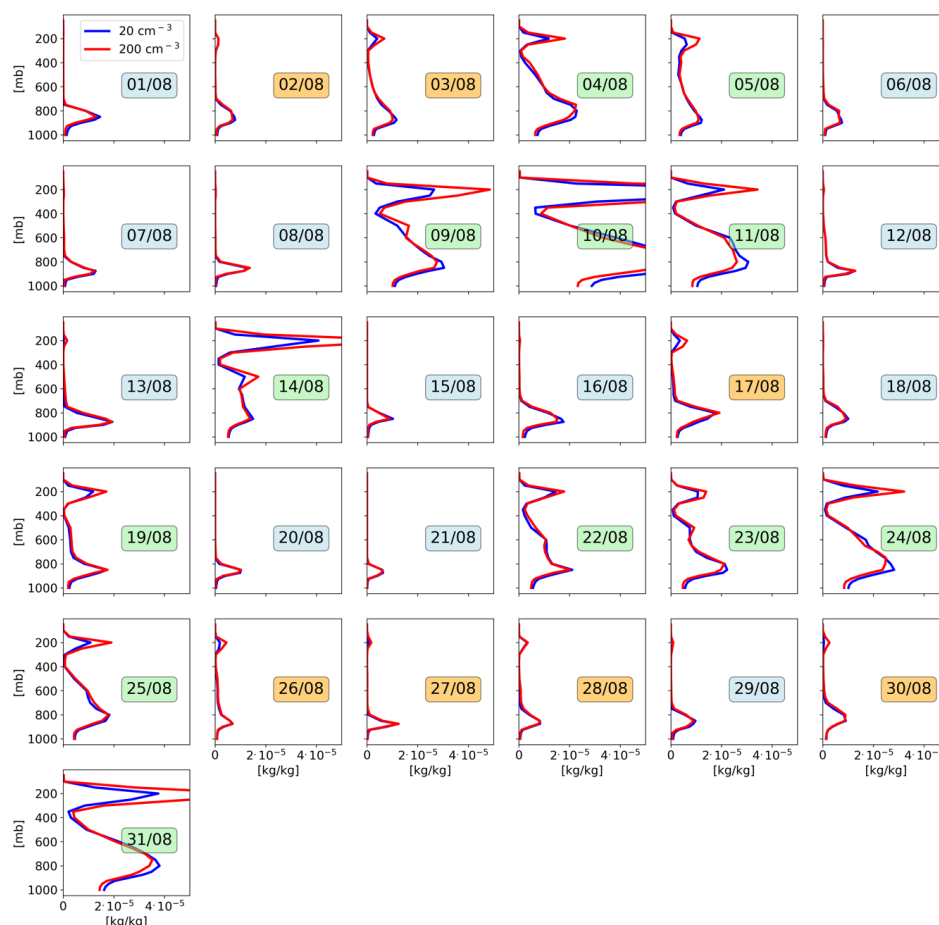
	Mean NARVAL 1	Mean NARVAL 2	p -value t -test
CF [%]	57.2 ± 13.7	52.3 ± 13.4	0.16
LWP [kg/m^2]	$4.8 \cdot 10^{-2} \pm 2.8 \cdot 10^{-2}$	$4.5 \cdot 10^{-2} \pm 2.2 \cdot 10^{-2}$	0.66
IWP [kg/m^2]	$5.7 \cdot 10^{-3} \pm 1.1 \cdot 10^{-2}$	$1.2 \cdot 10^{-2} \pm 2.4 \cdot 10^{-2}$	0.19
LP [W/m^2]	43.8 ± 47.8	52.2 ± 78.2	0.6
LTS [K]	13.9 ± 1.4	13.1 ± 0.7	$7 \cdot 10^{-3}$
$F_{\text{LW}}^{\text{TOA}}$ [W/m^2]	-254.2 ± 21.2	-251.7 ± 23.5	0.66
$F_{\text{SW}}^{\text{TOA}}$ [W/m^2]	241.7 ± 22.5	321.9 ± 26.4	$1.4 \cdot 10^{-18}$
Q_R [W/m^2]	-129.2 ± 17.8	-107.8 ± 21.7	$9.8 \cdot 10^{-5}$

Figures 3 and 4 present vertical profiles of the total water (liquid and ice) mixing ratio from the different simulations during NARVAL 2 (August 2016) and NARVAL 1 (December 2013),



172 respectively. Generally, during the winter month (NARVAL 1) the clouds are shallower than
 173 in the summer month (NARVAL 2), although there is significant variability. This is expected
 174 due to the seasonality of the ITCZ location (Stevens et al., 2016). The simulated days are
 175 manually separated to three different cloud regimes based on the domain and time mean total
 176 water mixing ratio vertical profiles. The cloud regimes considered here are: shallow clouds
 177 (shallow-cloud dominated days), two-layer clouds (shallow cloud layer and a cirrus cloud
 178 layer) and deep clouds (deep-cloud dominated days).

179



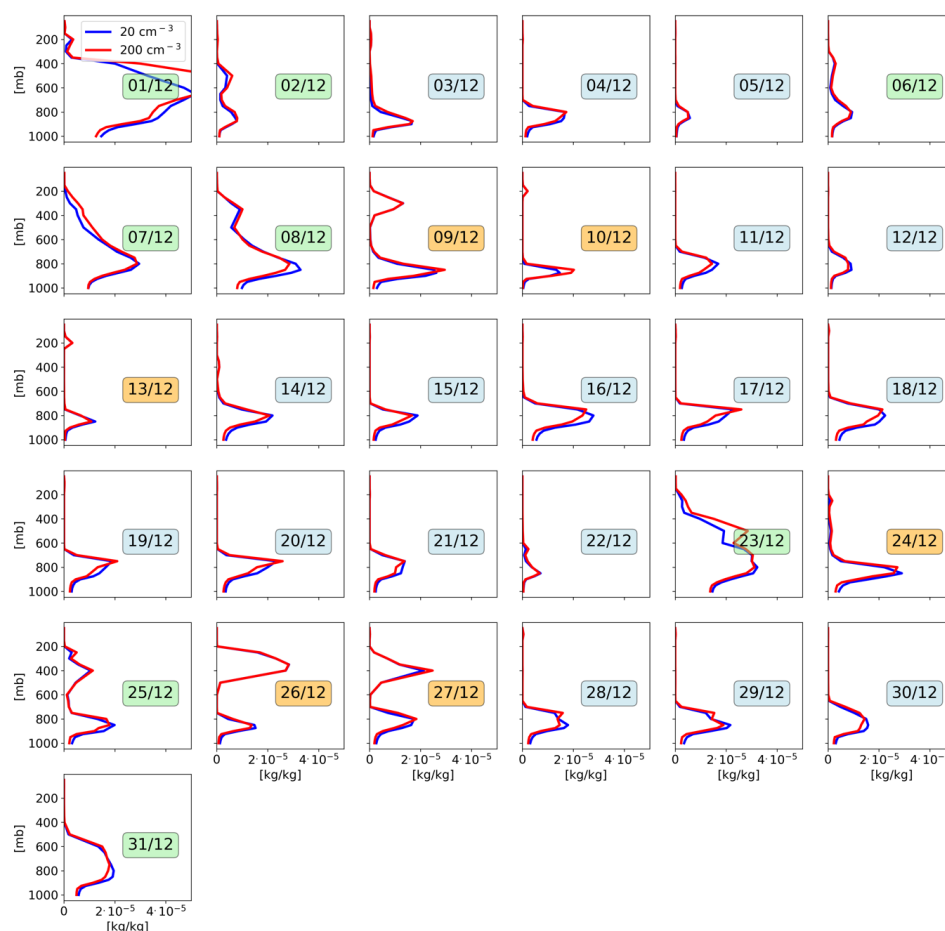
180

181 **Figure 3.** Mean (time and space) vertical profiles of the total water (liquid and ice) mixing ratio in each
 182 simulation (each last for 24 hours) for the NARVAL 2 month (August 2016). Blue: clean conditions (20 cm^{-3} ;
 183 3), red: polluted conditions (200 cm^{-3}). The simulated days are separated into three different cloud regimes:
 184 shallow clouds (blue date box), two-layer clouds (shallow cloud layer and a cirrus cloud layer – orange date
 185 box) and deep clouds (green date box).

186



187



188

189 **Figure 4. Same as Fig. 3 but for the NARVAL 1 month (December 2013).**

190

191 Figure 5 presents histograms of aerosol effects (polluted minus clean) for the different
 192 simulations. The distribution of changes in cloud fraction (Fig. 5a) demonstrate small mean
 193 values for both months (-0.3% and 0.1% for the winter and summer month, respectively) which
 194 is slightly more skewed to positive values in the summer. Examining the significance of these
 195 trends with a t-test demonstrates that only the winter month response is statistically significant
 196 (Table 2). The CDNC effect on the liquid water path (LWP; Fig. 5b) and the ice water path
 197 (IWP; Fig. 5c) is shown to be almost entirely positive (or zero) in both months and differs from
 198 zero in a statistically significant manner. The mean change in precipitation (Fig. 5d) is small
 199 and negative (slightly more negative during the winter month). However, during the summer



month it is not statistically significant and can be either positive or negative. We note that the mean precipitation decreases during the winter month (which is statistically significant) is small and equivalent to 0.07 mm/day (-1.8 W/m^2). Increasing CDNC systematically decreases LTS (Fig. 5e), representing deepening of the boundary layer (Dagan et al., 2016; Lebo and Morrison, 2014; Seifert et al., 2015; Stevens and Feingold, 2009). This trend is statistically significant for both months (Table 2).

The CDNC effect on F_{LW}^{TOA} is positive and small (average of 0.24 W/m^2) in the winter month (but still statistically significant) and larger (average of 2.16 W/m^2) in the summer month (Fig. 5f – positive flux downwards), primarily due to an increase in ice water content under polluted conditions (see also Figs. 3, 4 and 5c). We previously showed that an increase in CDNC drives an increase in the ice content at the upper troposphere and hence a reduction in the outgoing LW radiation (Dagan et al., 2019); here we show that this trend is statistically significant (Fig. 5c). However, during the winter, when deep convective clouds are less abundant and the atmosphere is more stable, the LW flux is less affected.

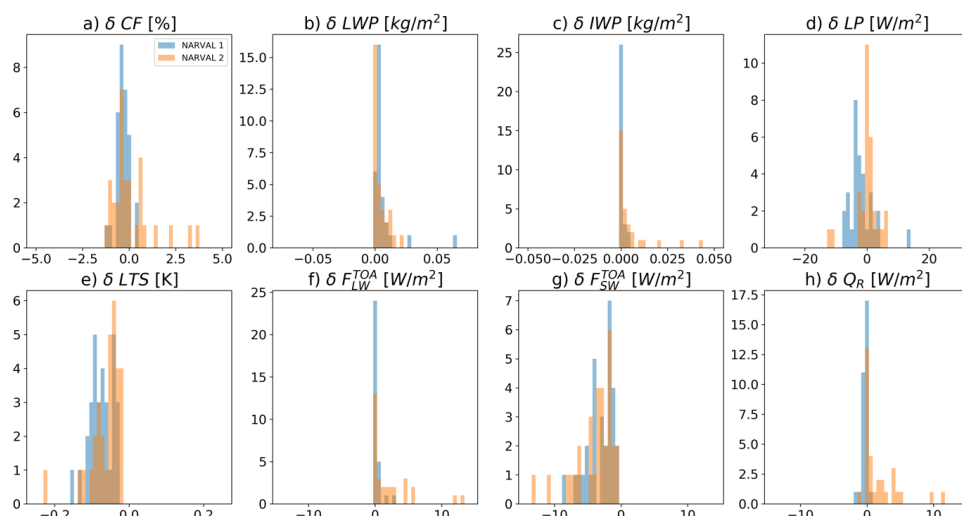
The CDNC effect on F_{SW}^{TOA} is always negative (Fig. 5g) and is on average -3.6 W/m^2 and -3.8 W/m^2 in the winter and summer month, respectively (the difference between the two months is not statistically significant; however, both differ from zero in a statistically significant manner – Table 2). The negative F_{SW}^{TOA} effect is caused mostly due to the Twomey effect (Twomey, 1977) and the LWP/IWP effect (Albrecht, 1989; Koren et al., 2010; Malavelle et al., 2017) (Figs. 5b and 5c), as the CF changes are small (Fig. 5a). For exploring the relative role of the Twomey and IWP/LWP effects, we ran all simulations again with the Twomey effect turned off. Without the Twomey effect the SW effect is reduced by up to a factor of 10 (-0.35 W/m^2 compared with -3.6 W/m^2 in the winter month, and -1.0 W/m^2 compared with -3.8 W/m^2 in the summer month). This demonstrates that the Twomey effect is the dominant factor underlying the F_{SW}^{TOA} changes. Radiative effects due to changes in ice size distribution are not considered due to uncertainties in the evolution of ice morphology. Accounting for this effect would further increase the relative role of the Twomey effect compare to the cloud adjustment effects (CF and LWP/IWP adjustments).

The change in the atmospheric column radiative warming term Q_R is shown to be small for the winter month (-0.26 W/m^2 on average) but much larger and positive for the summer month (1.8 W/m^2 on average). The increase in Q_R during the summer is caused due to the effect of deep, ice containing clouds on the outgoing LW flux (Fig. 5f). SW flux changes due to CDNC perturbations (Fig. 5g) have a much smaller effect on Q_R as the SW absorption of clouds is small (Dagan et al., 2019).



Examining the similarity between the response of the different properties to the CDNC perturbation in the two different months (Table 2) reveals that the responses of the IWP, F_{LW}^{TOA} , Q_R and F_{SW+LW}^{TOA} (the net TOA LW and SW effects – Fig. 10 below) are different in a statistically significant manner between the two months. As will be shown below, this is related to the response of the ice content.

239
 240



241
 242 **Figure 5. Histograms of the domain and time mean response of cloud and atmospheric properties to CDNC**
 243 **perturbation (polluted simulations minus clean simulations) for each day of the two months that were**
 244 **simulated. Blue represents the NARVAL 1 month (December 2013), while orange the NARVAL 2 month**
 245 **(August 2016). a) cloud fraction – CF, b) liquid water path - LWP, c) ice water path – IWP, d) precipitation**
 246 **latent heat flux - LP, e) lower tropospheric stability – LTS, f) top of atmosphere longwave flux - F_{LW}^{TOA} , g)**
 247 **top of atmosphere shortwave flux - F_{SW}^{TOA} , and h) atmospheric column radiative term - Q_R .**

248
 249
 250
 251
 252
 253
 254
 255
 256
 257



Table 2. Summary of monthly mean response of cloud and atmospheric properties (presented in Fig. 5) to the CDNC perturbation (polluted simulations minus clean simulations) ± 1 standard deviation for each month. In addition, the p-values of the two-sample independent t-test are presented, as well as the p-values for comparing the CDNC response in each month to zero. The p-values which demonstrate significant difference (<0.05) are presented in bold.

	Mean NARVAL 1	Mean NARVAL 2	p-value t-test	p-value one sample t- test compare to 0 - NARVAL 1	p-value one sample t- test compare to 0 - NARVAL 2
δCF [%]	-0.32 ± 0.31	0.11 ± 1.15	0.053	$8.1 \cdot 10^{-6}$	0.6
δLWP [kg/m ²]	$6.5 \cdot 10^{-3} \pm 1.2 \cdot 10^{-2}$	$4.0 \cdot 10^{-3} \pm 5.4 \cdot 10^{-3}$	0.3	$4.4 \cdot 10^{-3}$	$3.5 \cdot 10^{-4}$
δIWP [kg/m ²]	$5.6 \cdot 10^{-4} \pm 1.3 \cdot 10^{-3}$	$8.2 \cdot 10^{-3} \pm 1.9 \cdot 10^{-2}$	0.035	0.02	0.03
δLP [W/m ²]	-1.8 ± 4.1	-1.2 ± 7.0	0.7	0.02	0.37
δLTS [K]	-0.075 ± 0.031	-0.062 ± 0.042	0.18	$3.2 \cdot 10^{-14}$	$4.3 \cdot 10^{-9}$
δF_{LW}^{TOA} [W/m ²]	0.24 ± 0.60	2.16 ± 3.25	0.002	0.03	0.001
δF_{SW}^{TOA} [W/m ²]	-3.6 ± 3.5	-3.8 ± 2.9	0.8	$3.3 \cdot 10^{-6}$	$4.7 \cdot 10^{-8}$
δQ_R [W/m ²]	-0.26 ± 0.39	1.8 ± 2.8	$1.8 \cdot 10^{-4}$	$9.7 \cdot 10^{-4}$	$1.4 \cdot 10^{-3}$
δF_{SW+LW}^{TOA}	-3.36 ± 3.02	-1.67 ± 1.93	0.01	$1.1 \cdot 10^{-6}$	$5.1 \cdot 10^{-5}$

CDNC effect on different cloud regimes

For better understanding the trend demonstrated in Fig. 5 and Table 2, we split the simulated days into different dominant cloud types/regimes (see Figs. 3 and 4). Figures 6 and 7 present histograms of the same atmospheric properties presented in Fig. 2 but separated by different cloud regimes – shallow clouds, two-layer clouds (shallow clouds with cirrus cloud layer above), and deep clouds. These figures demonstrate that the cloud fraction, LWP, IWP, precipitation, F_{LW}^{TOA} and Q_R are generally higher on days dominated by deep-clouds as compared to days dominated by shallow clouds, while the LTS and F_{SW}^{TOA} are lower in the deep-cloud dominated days compared to shallow-cloud dominated days (with the two-layer cloud days generally in-between them). The separation into different cloud regimes also demonstrates that more deep-cloud days are occurring during the summer month as compared to the winter month (12 compare to 8) and that the deep clouds during summer are deeper and contain more water.

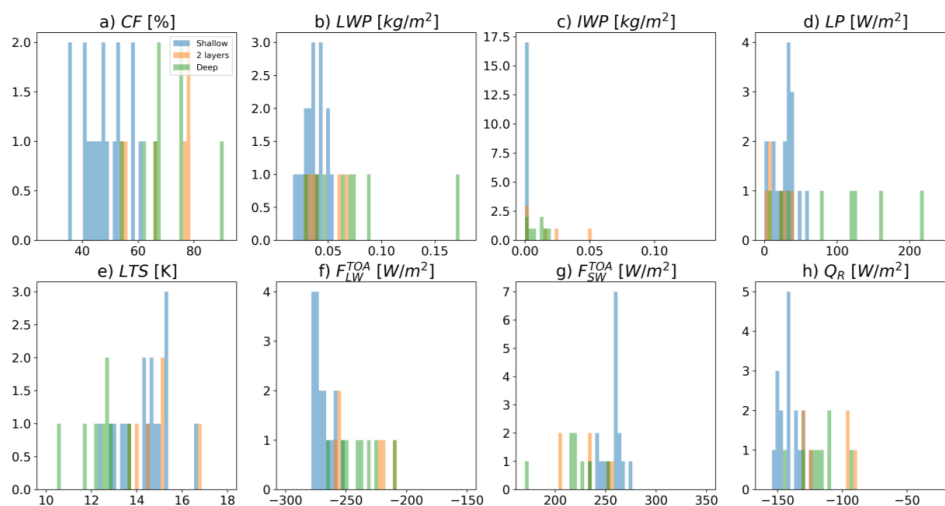


Figure 6. Histograms of mean (time and space) cloud and atmospheric properties for the base simulations with $\text{CDNC} = 20 \text{ cm}^{-3}$ (clean simulations) for each day of the NARVAL 1 month (December 2013) separated into different cloud regimes: shallow clouds (blue), two-layer clouds (shallow clouds with cirrus clouds layer above - orange), and deep clouds (green). a) cloud fraction – CF, b) liquid water path - LWP, c) ice water path – IWP, d) precipitation latent heat flux - LP, e) lower tropospheric stability – LTS, f) top of atmosphere longwave flux - $F_{\text{LW}}^{\text{TOA}}$, g) top of atmosphere shortwave flux - $F_{\text{SW}}^{\text{TOA}}$, and h) atmospheric column radiative term - Q_R .

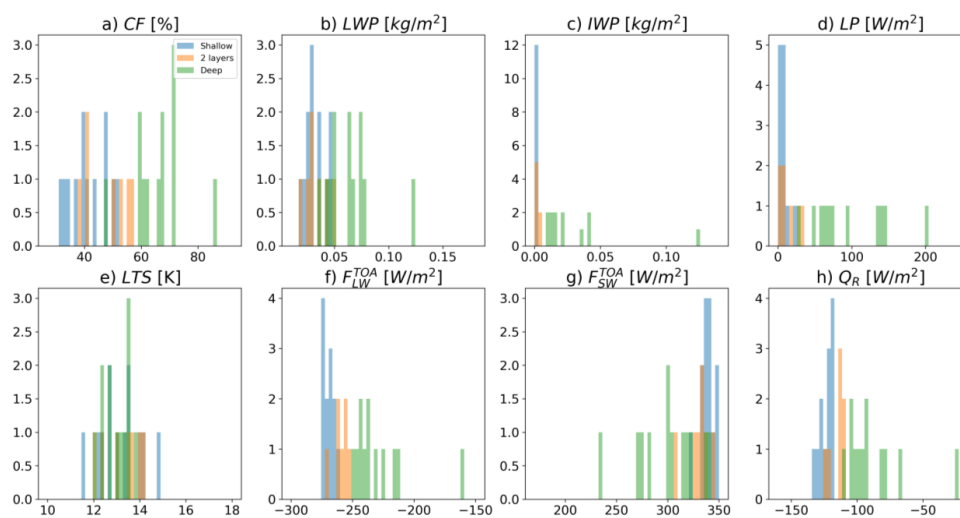
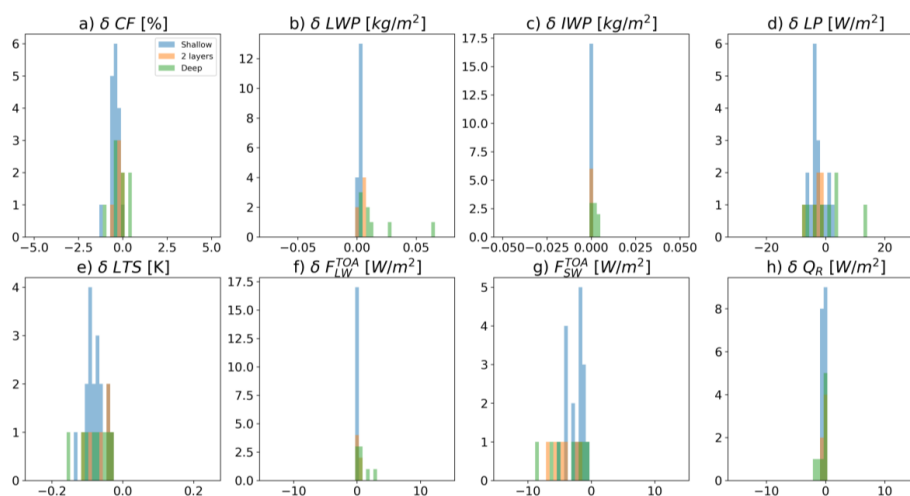


Figure 7. Same as Fig. 6 but for the NARVAL 2 month (August 2016).



Examining the response of the different cloud regimes to the CDNC perturbation (Figs. 8 and 9) demonstrates that the response of the cloud fraction, LWP, IWP and F_{LW}^{TOA} in the deep-cloud days is generally more positive, while the response of F_{LW}^{TOA} and LTS is generally more negative. These trends are more pronounced during the summer month as compared to the winter month. The response of Q_R is more positive in the deep-cloud dominated days in the summer month but does not show any different trend in the winter month. The precipitation response does not show any distinct different trend for the different cloud types in both months. The findings presented in Figs. 8 and 9 demonstrate that the IWP response in the deep-cloud dominated days is generally stronger in the summer month as compare to the winter month. The increase in the IWP with the increase in CDNC drives a reduction in F_{LW}^{TOA} and hence increase in Q_R (Dagan et al., 2019). We note that the largest difference between the two months emerges due to the stronger response of the ice content in the summer month as compared to the winter month. This fact can explain the statistically significant different response of the IWP, F_{LW}^{TOA} and Q_R shown in Table 2.

305
 306
 307

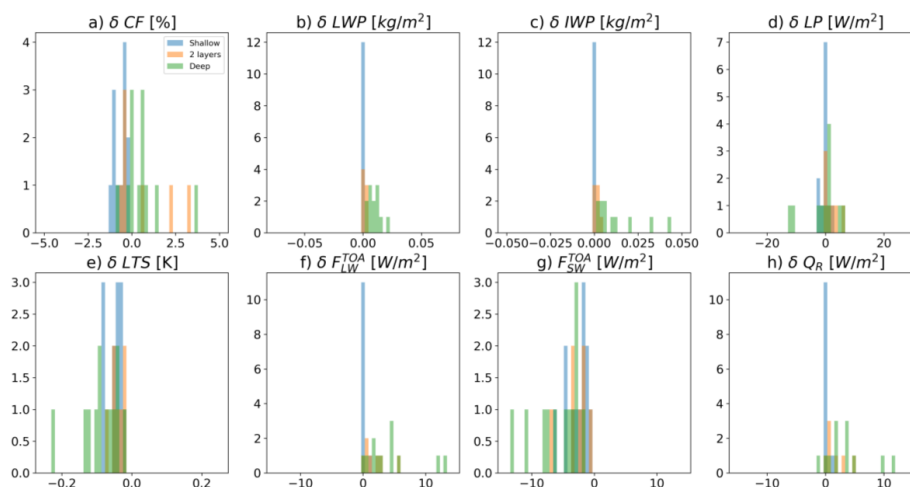


308

Figure 8. Histograms of the domain and time mean response of cloud and atmospheric properties to the CDNC perturbation (polluted simulations minus clean simulations) for each day of the NARVAL 1 month (December 2013) separated into the different cloud regimes: shallow clouds (blue), two-layer clouds (shallow clouds with cirrus clouds layer above - orange), and deep clouds (green). a) cloud fraction – CF, b) liquid water path - LWP, c) ice water path – IWP, d) precipitation latent heat flux - LP, e) lower tropospheric stability – LTS, f) top of atmosphere longwave flux - F_{LW}^{TOA} , g) top of atmosphere shortwave flux - F_{SW}^{TOA} , and h) atmospheric column radiative term - Q_R .



316
 317



318
 319

Figure 9. Same as Fig. 8 but for the NARVAL 2 month (August 2016).

320

321 The combined CDNC effect on the total net TOA radiation (F_{SW+LW}^{TOA}) is shown in Fig. 10. It
 322 demonstrates that during the winter month the effect on F_{SW+LW}^{TOA} is always negative and has a
 323 mean value of -3.4 W/m^2 . However, during the summer month, the mean effect is less negative
 324 (-1.7 W/m^2) and for some of the days it could even be positive due to the effect of the CDNC
 325 on the ice water content (Fig. 5 and Table 2). The difference between the two months in F_{SW+LW}^{TOA}
 326 is statistically significant (Table 2). We note that during the summer month all days for which
 327 $F_{SW+LW}^{TOA} \geq 0$ are deep-cloud dominated days, supporting the hypothesis that the difference
 328 between the different months are driven by the different response of the deep clouds, which are
 329 deeper and contain more water in the summer month.

330

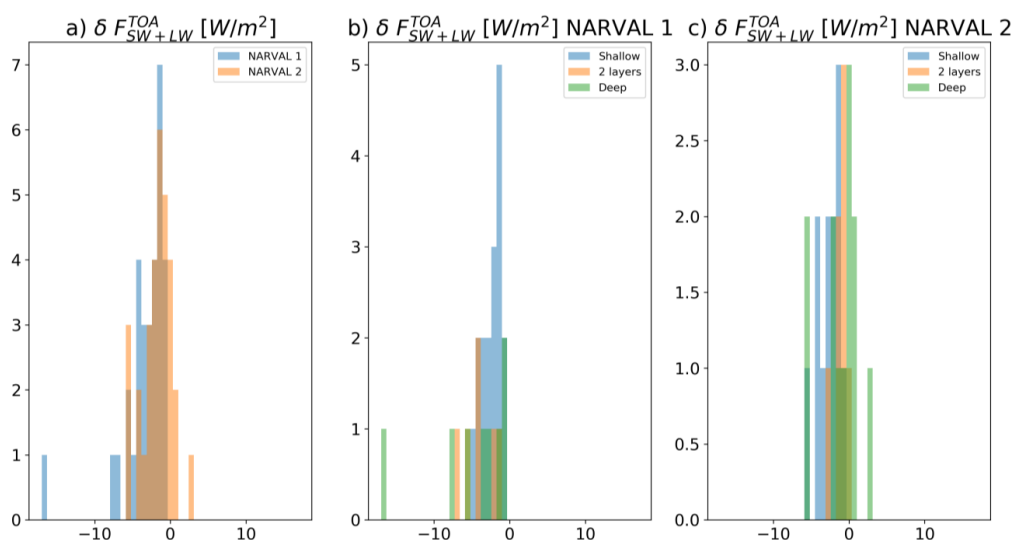


Figure 10. Histograms of the response of the net (shortwave + longwave) top of atmosphere radiative flux (F_{SW+LW}^{TOA}) to the CDNC perturbation (polluted simulations minus clean simulations) for each of the simulated days. In a) blue represents the NARVAL 1 month (December 2013), while orange the NARVAL 2 month (August 2016). In b) and c) the NARVAL 1 and the NARVAL 2 months are separated to the different cloud regimes: shallow clouds (blue), two-layer clouds (shallow clouds with cirrus clouds layer above - orange), and deep clouds (green).

Summary

Ensemble daily simulations over a region near Barbados for two separate month-long periods were conducted to investigate aerosol effects on cloud properties and the atmospheric energy budget. For each day, two simulations were conducted with low and high CDNC representing clean and polluted conditions, respectively. These simulations are used to distinguish between properties that are robustly affected by changes in CDNC and those that are not. For example, we have shown that, for the entire set of simulations (62 different days), an increase in CDNC always drives a reduction in the lower tropospheric stability (Fig. 5). In addition, F_{SW}^{TOA} is always reduced by an increase in CDNC, representing more SW reflection. However, changes in cloud fraction or precipitation are not as robustly affected, and, despite the fact that for a given day they could be large, on average they are not distinguishable from zero (at least for the summer month). However, we note that the aerosol response we present here may be underestimate due to the effect of the fixed boundary conditions and hence is estimated as the lower bound. In addition, the use of two month-long periods, covering different seasons dominated by different meteorological conditions and cloud type, demonstrate again (Altartatz et al.,



2014; Lee et al., 2009; Mülmenstädt and Feingold, 2018; van den Heever et al., 2011; Rosenfeld et al., 2013; Glassmeier and Lohmann, 2016; Gryspeerdt and Stier, 2012; Dagan et al., 2015a), that the aerosol effect on clouds is strongly dependent on cloud regimes and meteorological conditions. For our simulations we demonstrate that the top of atmosphere net radiative effect is twice as large during the winter month as compared to the summer month (Fig. 10). To better understand these differences we have split the simulated days into three different dominant cloud regimes. The results demonstrate that most of the differences in the response to CDNC increases between the two months are driven by the response of the ice content in deep convective clouds. During the summer month, the atmosphere is less stable and the deep convective clouds in the base-line simulations are more abundant, reach higher levels in the atmosphere and contain more water. These more developed clouds respond stronger to the CDNC perturbations and develop more ice content than the shallower clouds during the winter month. The increased ice is driven by increase in mass flux to the upper levels. The added ice content reduces the outgoing LW flux at the TOA and hence compensates some of the SW effect, which itself is similar between the summer and winter months. Our results highlight the need to use large ensembles of initial conditions for cloud-aerosol interaction studies, even in large domain simulations, and suggest that caution is needed when trying to draw conclusions from a single case-study experiments and short-term observations.

Author contributions. G. D. carried out the simulations and analyses presented. P. S. assisted with the design and interpretation of the analyses. G.D. prepared the manuscript with contributions from P.S.

Acknowledgements:

This research was supported by the European Research Council (ERC) project constRaining the EffeCts of Aerosols on Precipitation (RECAP) under the European Union's Horizon 2020 research and innovation programme with grant agreement No 724602. The simulations were performed using the ARCHER UK National Supercomputing Service. We acknowledge MPI, DWD and DKRZ for the NARVAL simulations.

References

Albrecht, B. A.: Aerosols, cloud microphysics, and fractional cloudiness, Science (New York, NY), 245, 1227, 1989.



- 389 Altaratz, O., Koren, I., Remer, L., and Hirsch, E.: Review: Cloud invigoration by aerosols—
 390 Coupling between microphysics and dynamics, *Atmospheric Research*, 140, 38-60, 2014.
- 391 Bellouin, N., Quaas, J., Gryspeerdt, E., Kinne, S., Stier, P., Watson-Parris, D., Boucher, O.,
 392 Carslaw, K., Christensen, M., and Daniau, A.-L.: Bounding aerosol radiative forcing of climate
 393 change, *Reviews of Geophysics*, 2019.
- 394 Boucher, O., Randall, D., Artaxo, P., Bretherton, C., Feingold, G., Forster, P., Kerminen, V.,
 395 Kondo, Y., Liao, H., and Lohmann, U.: Clouds and aerosols, *Climate Change*, 571-657, 2013.
- 396 Chen, Q., Koren, I., Altaratz, O., Heiblum, R. H., Dagan, G., and Pinto, L.: How do changes
 397 in warm-phase microphysics affect deep convective clouds?, *Atmospheric Chemistry and*
 398 *Physics*, 17, 9585-9598, 2017.
- 399 Christensen, M. W., Chen, Y. C., and Stephens, G. L.: Aerosol indirect effect dictated by liquid
 400 clouds, *Journal of Geophysical Research: Atmospheres*, 121, 2016.
- 401 Clough, S., Shephard, M., Mlawer, E., Delamere, J., Iacono, M., Cady-Pereira, K., Boukabara,
 402 S., and Brown, P.: Atmospheric radiative transfer modeling: a summary of the AER codes,
 403 *Journal of Quantitative Spectroscopy and Radiative Transfer*, 91, 233-244, 2005.
- 404 Dagan, G., Koren, I., and Altaratz, O.: Competition between core and periphery-based
 405 processes in warm convective clouds—from invigoration to suppression, *Atmospheric*
 406 *Chemistry and Physics*, 15, 2749-2760, 2015a.
- 407 Dagan, G., Koren, I., and Altaratz, O.: Aerosol effects on the timing of warm rain processes,
 408 *Geophysical Research Letters*, 42, 4590-4598, 10.1002/2015GL063839, 2015b.
- 409 Dagan, G., Koren, I., Altaratz, O., and Heiblum, R. H.: Aerosol effect on the evolution of the
 410 thermodynamic properties of warm convective cloud fields, *Scientific Reports*, 38769,
 411 <https://doi.org/10.1038/srep38769>, 2016.
- 412 Dagan, G., Koren, I., Altaratz, O., and Heiblum, R. H.: Time-dependent, non-monotonic
 413 response of warm convective cloud fields to changes in aerosol loading, *Atmos. Chem. Phys.*,
 414 17, 7435-7444, 10.5194/acp-17-7435-2017, 2017.
- 415 Dagan, G., Koren, I., and Altaratz, O.: Quantifying the effect of aerosol on vertical velocity
 416 and effective terminal velocity in warm convective clouds, *Atmospheric Chemistry and*
 417 *Physics*, 18, 6761-6769, 2018a.
- 418 Dagan, G., Koren, I., Kostinski, A., and Altaratz, O.: Organization and oscillations in simulated
 419 shallow convective clouds, *Journal of Advances in Modeling Earth Systems*, 2018b.
- 420 Dagan, G., Stier, P., Christensen, M., Cioni, G., Klocke, D., and Seifert, A.: Atmospheric
 421 energy budget response to idealized aerosol perturbation in tropical cloud systems, *Atmos.*
 422 *Chem. Phys. Discuss.*, <https://doi.org/10.5194/acp-2019-813>, in review, 2019.



- 423 Fan, J., Zhang, R., Li, G., and Tao, W.-K.: Effects of aerosols and relative humidity on cumulus
 424 clouds, *Journal of Geophysical Research-Atmospheres*, 112, 10.1029/2006jd008136, 2007.
- 425 Fan, J., Yuan, T., Comstock, J. M., Ghan, S., Khain, A., Leung, L. R., Li, Z., Martins, V. J.,
 426 and Ovchinnikov, M.: Dominant role by vertical wind shear in regulating aerosol effects on
 427 deep convective clouds, *Journal of Geophysical Research-Atmospheres*, 114,
 428 10.1029/2009jd012352, 2009.
- 429 Glassmeier, F., and Lohmann, U.: Constraining precipitation susceptibility of warm-, ice-, and
 430 mixed-phase clouds with microphysical equations, *Journal of the Atmospheric Sciences*, 73,
 431 5003-5023, 2016.
- 432 Grabowski, W. W.: Untangling microphysical impacts on deep convection applying a novel
 433 modeling methodology, *Journal of the Atmospheric Sciences*, 72, 2446-2464, 2015.
- 434 Gryspeerdt, E., and Stier, P.: Regime- based analysis of aerosol- cloud interactions,
 435 *Geophysical Research Letters*, 39, 2012.
- 436 Gryspeerdt, E., Goren, T., Sourdeval, O., Quaas, J., Mülmenstädt, J., Dipu, S., Unglaub, C.,
 437 Gettelman, A., and Christensen, M.: Constraining the aerosol influence on cloud liquid water
 438 path, *Atmospheric Chemistry and Physics*, 19, 5331-5347, 2019.
- 439 Gustafson Jr, W., and Vogelmann, A.: LES ARM Symbiotic Simulation and Observation
 440 (LASSO) Implementation Strategy, DOE Office of Science Atmospheric Radiation
 441 Measurement (ARM) Program ..., 2015.
- 442 Gustafson, W. I., Vogelmann, A. M., Cheng, X., Endo, S., Krishna, B., Li, Z., Toto, T., and
 443 Xiao, H.: Description of the LASSO Alpha 2 Release, DOE Office of Science Atmospheric
 444 Radiation Measurement (ARM) Program ..., 2017.
- 445 Heikenfeld, M., White, B., Labbouz, L., and Stier, P.: Aerosol effects on deep convection: the
 446 propagation of aerosol perturbations through convective cloud microphysics, *Atmospheric*
 447 *Chemistry and Physics*, 19, 2601-2627, 2019.
- 448 Iacono, M. J., Delamere, J. S., Mlawer, E. J., Shephard, M. W., Clough, S. A., and Collins, W.
 449 D.: Radiative forcing by long- lived greenhouse gases: Calculations with the AER radiative
 450 transfer models, *Journal of Geophysical Research: Atmospheres*, 113, 2008.
- 451 Kalina, E. A., Friedrich, K., Morrison, H., and Bryan, G. H.: Aerosol effects on idealized
 452 supercell thunderstorms in different environments, *Journal of the Atmospheric Sciences*, 71,
 453 4558-4580, 2014.
- 454 Khain, A., Rosenfeld, D., and Pokrovsky, A.: Aerosol impact on the dynamics and
 455 microphysics of deep convective clouds, *Quarterly Journal of the Royal Meteorological*
 456 *Society*, 131, 2639-2663, 10.1256/qj.04.62, 2005.



- 457 Khain, A. P., BenMoshe, N., and Pokrovsky, A.: Factors determining the impact of aerosols
 458 on surface precipitation from clouds: An attempt at classification, *Journal of the Atmospheric*
 459 *Sciences*, 65, 1721-1748, 10.1175/2007jas2515.1, 2008.
- 460 Klepp, C., Ament, F., Bakan, S., Hirsch, L., and Stevens, B.: The NARVAL Campaign Report,
 461 2014.
- 462 Klocke, D., Brueck, M., Hohenegger, C., and Stevens, B.: Rediscovery of the doldrums in
 463 storm-resolving simulations over the tropical Atlantic, *Nature Geoscience*, 10, 891, 2017.
- 464 Koren, I., Kaufman, Y. J., Rosenfeld, D., Remer, L. A., and Rudich, Y.: Aerosol invigoration
 465 and restructuring of Atlantic convective clouds, *Geophysical Research Letters*, 32,
 466 10.1029/2005gl023187, 2005.
- 467 Koren, I., Remer, L. A., Altaratz, O., Martins, J. V., and Davidi, A.: Aerosol-induced changes
 468 of convective cloud anvils produce strong climate warming, *Atmospheric Chemistry and*
 469 *Physics*, 10, 5001-5010, 10.5194/acp-10-5001-2010, 2010.
- 470 Koren, I., Dagan, G., and Altaratz, O.: From aerosol-limited to invigoration of warm
 471 convective clouds, *science*, 344, 1143-1146, 2014.
- 472 Lebo, Z. J., and Morrison, H.: Dynamical effects of aerosol perturbations on simulated
 473 idealized squall lines, *Monthly Weather Review*, 142, 991-1009, 2014.
- 474 Lee, S. S., Donner, L. J., and Phillips, V. T. J.: Sensitivity of aerosol and cloud effects on
 475 radiation to cloud types: comparison between deep convective clouds and warm stratiform
 476 clouds over one-day period, *Atmospheric Chemistry and Physics*, 9, 2555-2575, 2009.
- 477 Levin, Z., and Cotton, W. R.: Aerosol pollution impact on precipitation: A scientific review,
 478 Springer, 2009.
- 479 Liu, H., Guo, J., Koren, I., Altaratz, O., Dagan, G., Wang, Y., Jiang, J. H., Zhai, P., and Yung,
 480 Y. L.: Non-Monotonic Aerosol Effect on Precipitation in Convective Clouds over Tropical
 481 Oceans, *Scientific Reports*, 9, 7809, 2019.
- 482 Malavelle, F. F., Haywood, J. M., Jones, A., Gettelman, A., Clarisse, L., Bauduin, S., Allan,
 483 R. P., Karset, I. H. H., Kristjánsson, J. E., and Oreopoulos, L.: Strong constraints on aerosol–
 484 cloud interactions from volcanic eruptions, *Nature*, 546, 485, 2017.
- 485 Medeiros, B., and Nuijens, L.: Clouds at Barbados are representative of clouds across the trade
 486 wind regions in observations and climate models, *Proceedings of the National Academy of*
 487 *Sciences*, 113, E3062-E3070, 2016.
- 488 Mlawer, E. J., Taubman, S. J., Brown, P. D., Iacono, M. J., and Clough, S. A.: Radiative
 489 transfer for inhomogeneous atmospheres: RRTM, a validated correlated- k model for the
 490 longwave, *Journal of Geophysical Research: Atmospheres*, 102, 16663-16682, 1997.



- 491 Mülmenstädt, J., and Feingold, G.: The Radiative Forcing of Aerosol–Cloud Interactions in
 492 Liquid Clouds: Wrestling and Embracing Uncertainty, *Current Climate Change Reports*, 4, 23–
 493 40, 2018.
- 494 Rosenfeld, D., Lohmann, U., Raga, G. B., O'Dowd, C. D., Kulmala, M., Fuzzi, S., Reissell, A.,
 495 and Andreae, M. O.: Flood or drought: How do aerosols affect precipitation?, *Science*, 321,
 496 1309–1313, 10.1126/science.1160606, 2008.
- 497 Rosenfeld, D., Wood, R., Donner, L. J., and Sherwood, S. C.: Aerosol cloud-mediated radiative
 498 forcing: highly uncertain and opposite effects from shallow and deep clouds, in: *Climate*
 499 *Science for Serving Society*, Springer, 105–149, 2013.
- 500 Rosenfeld, D., Zhu, Y., Wang, M., Zheng, Y., Goren, T., and Yu, S.: Aerosol-driven droplet
 501 concentrations dominate coverage and water of oceanic low-level clouds, *Science*, 363,
 502 eaav0566, 2019.
- 503 Rothenberg, D., Avramov, A., and Wang, C.: On the representation of aerosol activation and
 504 its influence on model-derived estimates of the aerosol indirect effect, *Atmos. Chem. Phys.*, 18,
 505 7961–7983, 2018.
- 506 Seifert, A., and Beheng, K.: A two-moment cloud microphysics parameterization for mixed-
 507 phase clouds. Part 2: Maritime vs. continental deep convective storms, *Meteorology and*
 508 *Atmospheric Physics*, 92, 67–82, 2006a.
- 509 Seifert, A., and Beheng, K. D.: A two-moment cloud microphysics parameterization for mixed-
 510 phase clouds. Part 1: Model description, *Meteorology and atmospheric physics*, 92, 45–66,
 511 2006b.
- 512 Seifert, A., Heus, T., Pincus, R., and Stevens, B.: Large-eddy simulation of the transient and
 513 near-equilibrium behavior of precipitating shallow convection, *Journal of Advances in*
 514 *Modeling Earth Systems*, 2015.
- 515 Stevens, B., and Feingold, G.: Untangling aerosol effects on clouds and precipitation in a
 516 buffered system, *Nature*, 461, 607–613, 10.1038/nature08281, 2009.
- 517 Stevens, B., Farrell, D., Hirsch, L., Jansen, F., Nuijens, L., Serikov, I., Brüggemann, B., Forde,
 518 M., Linne, H., and Lonitz, K.: The Barbados Cloud Observatory: Anchoring investigations of
 519 clouds and circulation on the edge of the ITCZ, *Bulletin of the American Meteorological*
 520 *Society*, 97, 787–801, 2016.
- 521 Stevens, B., Ament, F., Bony, S., Crewell, S., Ewald, F., Gross, S., Hansen, A., Hirsch, L.,
 522 Jacob, M., and Kölling, T.: A high-altitude long-range aircraft configured as a cloud
 523 observatory—the NARVAL expeditions, *Bulletin of the American Meteorological Society*,
 524 2019.



525 Storelvmo, T., Hoose, C., and Eriksson, P.: Global modeling of mixed- phase clouds: The
 526 albedo and lifetime effects of aerosols, *Journal of Geophysical Research: Atmospheres*, 116,
 527 2011.

528 Tao, W.-K., Chen, J.-P., Li, Z., Wang, C., and Zhang, C.: Impact of aerosols on convective
 529 clouds and precipitation, *Reviews of Geophysics*, 50, RG2001, 2012.

530 Twomey, S.: The influence of pollution on the shortwave albedo of clouds, *Journal of the*
 531 *atmospheric sciences*, 34, 1149-1152, 1977.

532 van den Heever, S. C., Stephens, G. L., and Wood, N. B.: Aerosol Indirect Effects on Tropical
 533 Convection Characteristics under Conditions of Radiative-Convective Equilibrium, *Journal of*
 534 *the Atmospheric Sciences*, 68, 699-718, 10.1175/2010jas3603.1, 2011.

535 Zängl, G., Reinert, D., Rípodas, P., and Baldauf, M.: The ICON (ICOsahedral Non-
 536 hydrostatic) modelling framework of DWD and MPI- M: Description of the non- hydrostatic
 537 dynamical core, *Quarterly Journal of the Royal Meteorological Society*, 141, 563-579, 2015.

538

539